Reflective afocal broadband adaptive optics scanning ophthalmoscope

Alfredo Dubra[1,*] and Yusufu Sulai[2]

[1]*Flaum Eye Institute, University of Rochester, Rochester, NY, 14642-0314, USA*
[2]*The Institute of Optics, University of Rochester, Rochester, NY, 14627, USA*
**adubra@cvs.rochester.edu*

Abstract: A broadband adaptive optics scanning ophthalmoscope (BAOSO) consisting of four afocal telescopes, formed by pairs of off-axis spherical mirrors in a non-planar arrangement, is presented. The non-planar folding of the telescopes is used to simultaneously reduce pupil and image plane astigmatism. The former improves the adaptive optics performance by reducing the root-mean-square (RMS) of the wavefront and the beam wandering due to optical scanning. The latter provides diffraction limited performance over a 3 diopter (D) vergence range. This vergence range allows for the use of any broadband light source(s) in the 450-850 nm wavelength range to simultaneously image any combination of retinal layers. Imaging modalities that could benefit from such a large vergence range are optical coherence tomography (OCT), multi- and hyper-spectral imaging, single- and multi-photon fluorescence. The benefits of the non-planar telescopes in the BAOSO are illustrated by resolving the human foveal photoreceptor mosaic in reflectance using two different superluminescent diodes with 680 and 796 nm peak wavelengths, reaching the eye with a vergence of 0.76 D relative to each other.

OCIS codes: (110.1080) Active or adaptive optics; (080.4035) Mirror system design; (170.4460) Ophthalmic optics and devices; (170.4470) Ophthalmology.

References and links

1. E. A. Rossi, M. Chung, A. Dubra, J. J. Hunter, W. H. Merigan, and D. R. Williams, "Imaging retinal mosaics in the living eye," Eye (Lond.) **25**(3), 301–308 (2011).
2. J. Liang, D. R. Williams, and D. T. Miller, "Supernormal vision and high-resolution retinal imaging through adaptive optics," J. Opt. Soc. Am. A **14**(11), 2884–2892 (1997).
3. J. Rha, R. S. Jonnal, K. E. Thorn, J. Qu, Y. Zhang, and D. T. Miller, "Adaptive optics flood-illumination camera for high speed retinal imaging," Opt. Express **14**(10), 4552–4569 (2006).
4. B. Hermann, E. J. Fernández, A. Unterhuber, H. Sattmann, A. F. Fercher, W. Drexler, P. M. Prieto, and P. Artal, "Adaptive-optics ultrahigh-resolution optical coherence tomography," Opt. Lett. **29**(18), 2142–2144 (2004).
5. Y. Zhang, J. T. Rha, R. S. Jonnal, and D. T. Miller, "Adaptive optics parallel spectral domain optical coherence tomography for imaging the living retina," Opt. Express **13**(12), 4792–4811 (2005).
6. R. J. Zawadzki, S. M. Jones, S. S. Olivier, M. T. Zhao, B. A. Bower, J. A. Izatt, S. Choi, S. Laut, and J. S. Werner, "Adaptive-optics optical coherence tomography for high-resolution and high-speed 3D retinal in vivo imaging," Opt. Express **13**(21), 8532–8546 (2005).
7. D. Merino, C. Dainty, A. Bradu, and A. G. Podoleanu, "Adaptive optics enhanced simultaneous en-face optical coherence tomography and scanning laser ophthalmoscopy," Opt. Express **14**(8), 3345–3353 (2006).
8. A. Roorda, F. Romero-Borja, W. Donnelly Iii, H. Queener, T. J. Hebert, and M. C. W. Campbell, "Adaptive optics scanning laser ophthalmoscopy," Opt. Express **10**(9), 405–412 (2002).
9. D. X. Hammer, R. D. Ferguson, C. E. Bigelow, N. V. Iftimia, T. E. Ustun, and S. A. Burns, "Adaptive optics scanning laser ophthalmoscope for stabilized retinal imaging," Opt. Express **14**(8), 3354–3367 (2006).
10. D. C. Gray, W. Merigan, J. I. Wolfing, B. P. Gee, J. Porter, A. Dubra, T. H. Twietmeyer, K. Ahamd, R. Tumbar, F. Reinholz, and D. R. Williams, "In vivo fluorescence imaging of primate retinal ganglion cells and retinal pigment epithelial cells," Opt. Express **14**(16), 7144–7158 (2006).
11. D. C. Chen, S. M. Jones, D. A. Silva, and S. S. Olivier, "High-resolution adaptive optics scanning laser ophthalmoscope with dual deformable mirrors," J. Opt. Soc. Am. A **24**(5), 1305–1312 (2007).
12. J. J. Hunter, B. Masella, A. Dubra, R. Sharma, L. Yin, W. H. Merigan, G. Palczewska, K. Palczewski, and D. R. Williams, "Images of photoreceptors in living primate eyes using adaptive optics two-photon ophthalmoscopy," Biomed. Opt. Express **2**(1), 139–148 (2011).

#143934 - $15.00 USD Received 10 Mar 2011; revised 22 Apr 2011; accepted 22 Apr 2011; pub. 27 May 2011

13. A. Gómez-Vieyra, A. Dubra, D. Malacara-Hernández, and D. R. Williams, "First-order design of off-axis reflective ophthalmic adaptive optics systems using afocal telescopes," Opt. Express **17**(21), 18906–18919 (2009).
14. E. J. Fernández, B. Hermann, B. Považay, A. Unterhuber, H. Sattmann, B. Hofer, P. K. Ahnelt, and W. Drexler, "Ultrahigh resolution optical coherence tomography and pancorrection for cellular imaging of the living human retina," Opt. Express **16**(15), 11083–11094 (2008).
15. R. J. Zawadzki, B. Cense, Y. Zhang, S. S. Choi, D. T. Miller, and J. S. Werner, "Ultrahigh-resolution optical coherence tomography with monochromatic and chromatic aberration correction," Opt. Express **16**(11), 8126–8143 (2008).
16. C. Torti, B. Považay, B. Hofer, A. Unterhuber, J. Carroll, P. K. Ahnelt, and W. Drexler, "Adaptive optics optical coherence tomography at 120,000 depth scans/s for non-invasive cellular phenotyping of the living human retina," Opt. Express **17**(22), 19382–19400 (2009).
17. B. Alamouti and J. Funk, "Retinal thickness decreases with age: an OCT study," Br. J. Ophthalmol. **87**(7), 899–901 (2003).
18. G. Smith and D. A. Atchison, *The Eye and Visual Optical Instrumentation* (Cambridge University Press, Cambridge, UK, 1997).
19. L. N. Thibos, M. Ye, X. Zhang, and A. Bradley, "The chromatic eye: a new reduced-eye model of ocular chromatic aberration in humans," Appl. Opt. **31**(19), 3594–3600 (1992).
20. E. Fernández, A. Unterhuber, P. Prieto, B. Hermann, W. Drexler, and P. Artal, "Ocular aberrations as a function of wavelength in the near infrared measured with a femtosecond laser," Opt. Express **13**(2), 400–409 (2005).
21. P. Bedggood, M. Daaboul, R. Ashman, G. Smith, and A. Metha, "Characteristics of the human isoplanatic patch and implications for adaptive optics retinal imaging," J. Biomed. Opt. **13**(2), 024008 (2008).
22. L. N. Thibos, X. Hong, A. Bradley, and X. Cheng, "Statistical variation of aberration structure and image quality in a normal population of healthy eyes," J. Opt. Soc. Am. A **19**(12), 2329–2348 (2002).
23. C. W. Oyster, *The Human Eye: Structure and Function* (Sinauer Associates Inc, Sunderland, Massachusetts, USA, 1999).
24. ANSI, "American National Standard for safe use of lasers (ANSI 136.1)," ANSI 136.1–2007 (The Laser Institute of America, 2007).
25. F. C. Delori, R. H. Webb, and D. H. Sliney; American National Standards Institute, "Maximum permissible exposures for ocular safety (ANSI 2000), with emphasis on ophthalmic devices," J. Opt. Soc. Am. A **24**(5), 1250–1265 (2007).
26. A. Dubra and Z. Harvey, "Registration of 2D images from fast scanning ophthalmic instruments," Lect. Notes Comput. Sci. **6204**, 60–71 (2010).
27. A. Dubra, A. Gómez-Vieyra, L. Díaz-Santana and Y. Sulai, "Optical design of clinical adaptive optics instruments for retinal imaging," in *Frontiers in Optics*, OSA Technical Digest, paper FTuB3.

1. Introduction

Ophthalmic adaptive optics (AO) instruments allow *in vivo* visualization of microscopic retinal features by compensating for the monochromatic aberrations of the eye [1]. Among the various imaging modalities demonstrated to date [2–12], AO scanning techniques provide the highest lateral and axial resolution. In order to achieve the classical lateral and axial resolution limits in scanning AO ophthalmoscopes the full unobstructed entrance pupil should be utilized to illuminate the retina. Furthermore, the numerical aperture of mammalian eyes is relatively low (approximately 0.25 in primates and up to 0.50 in rodents) and retinal reflectivity is extremely low (10^{-3}-10^{-4}). As a result, reflective imaging systems have been preferred over refractive ones, as they have the advantage of avoiding undesired reflections from refractive surfaces. Most scanning ophthalmic AO instruments use one or more afocal telescopes formed by pairs of spherical mirrors used in planar off-axis arrangements that are dominated by astigmatism. Gómez-Vieyra *et al.* [13] showed that by folding these reflective telescopes in a non-planar configuration, it is possible to completely cancel the astigmatism at one point in the field of view (FOV) either in the pupil or image conjugate planes. In their work, Gómez-Vieyra *et al.* also demonstrated that by folding two afocal telescopes in a prescribed manner, astigmatism in all pupil conjugate planes and the exit image plane can be cancelled at one point in the FOV. The remaining degree of freedom in the combination of two telescopes can be used to reduce coma, by rigidly rotating the second telescope with respect to the first.

Section 2 of this work illustrates how the non-planar folding of afocal telescopes reduces astigmatism in both pupil and image conjugate planes across a given field of view. Section 3 discusses the need for diffraction limited performance over a large range of vergences for simultaneous imaging of multiple retinal layers and/or the use of broadband sources. This is followed by a description of the optical design of a low-astigmatism BAOSO in Section 4. Section 5 presents images of human foveal photoreceptors using two different imaging

#143934 - $15.00 USD Received 10 Mar 2011; revised 22 Apr 2011; accepted 22 Apr 2011; pub. 27 May 2011

channels with different vergences, to illustrate the capabilities of such an instrument. Finally, the performance of the BAOSO is summarized in Section 6.

2. Non-planar folding of a reflective off-axis afocal telescope

Most reflective ophthalmic AO scanning instruments use off-axis afocal telescopes consisting of pairs of spherical mirrors to relay the planes conjugated to the pupil of the eye [6–11], and therefore their design deserves some discussion. Let us start by noting that because of the off-axis nature of such reflective telescopes, there is no rotational symmetry along any given axis. The natural choice for optical axis then becomes the principal ray corresponding to the image point on the center of the field of view in the image (i.e. retinal) plane. To date, most of these reflective telescopes have been implemented in a planar configuration, that is, by keeping the optical axis of each individual telescope contained in a plane [6–11]. When this is not the case, the telescope configuration will be described as non-planar, with the most extreme case being when the two planes defined by the reflections of the optical axis on the two spherical mirrors are orthogonal.

The dominant aberration degrading image quality in the planes conjugate to the retina in the planar configuration is astigmatism. By orienting a series of planar telescopes angled with respect to each other, one can significantly reduce this astigmatism, without the need to add additional compensating elements [10,11]. In this way, diffraction limited performance has been achieved over the desired FOV in the image plane, provided the angles of incidence on the spherical mirrors were small. Non-planar folding of the telescopes, however, offers much better performance in both image and pupil conjugate planes, as is illustrated next. Let us consider a pair of spherical mirrors with 800 mm radii of curvature, separated by the sum of their focal lengths, with the angle of incidence of the principal ray at the center of the FOV being 5° onto both mirrors. A steering mirror (optical scanner) is placed in the front focal plane of the first mirror, scanning a 2° square FOV. As a metric for the optical performance of this 1:1 telescope, the power mean with exponent 2 of the wavefront RMS at 9 points, uniformly distributed over the field of view is calculated. Figure 1 shows the corresponding spot diagrams in the planar and orthogonal configurations, as reported by the optical design program ZEMAX (Zemax Development Corporation, Bellevue, Washington, USA). The wavefront RMS values for the corresponding telescope configurations are $\lambda/13$ and $\lambda/59$ respectively, with $\lambda = 680$ nm. The spot diagrams of the planar configuration correspond to the circle of least confusion for the astigmatism component that is much larger than that of the orthogonal one. Remarkably, simply folding the telescope orthogonally reduced the wavefront RMS by more than a factor of 4. Irrespective of the RMS value itself, which is dependent on the parameters of each telescope, the FOV and the wavelength(s) considered, non-planar folding without increasing the angles of incidence will always reduce astigmatism. In

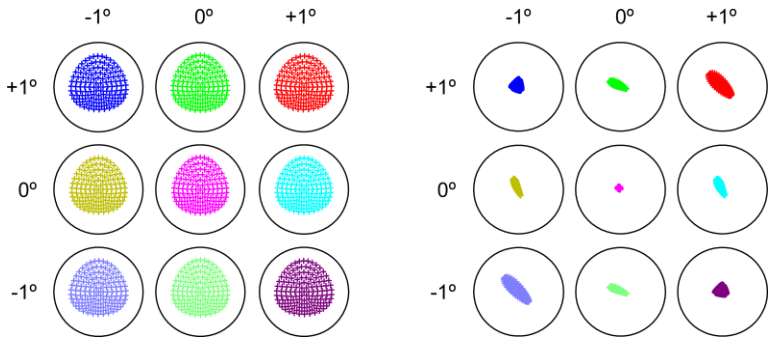

Fig. 1. Spot diagrams corresponding to the image plane of a 1:1 off-axis reflective afocal telescope that consists of two spherical mirrors with 800 mm radii of curvature in a planar configuration (left) and orthogonal configuration (right). The black circles correspond to the first minimum of the Airy disk.

#143934 - $15.00 USD Received 10 Mar 2011; revised 22 Apr 2011; accepted 22 Apr 2011; pub. 27 May 2011

particular, the orthogonal arrangement leads to the minimum overall astigmatism, and therefore the lowest wavefront RMS. Note that the residual astigmatism after non-planar folding varies linearly with the angle of incidence of the principal ray onto the spherical mirrors [13].

The non-planar folding of the telescope has an equally dramatic effect on the aberrations that affect the image quality at the back focal plane of the second spherical mirror, which in ophthalmic AO instruments would be conjugate to the pupil of the eye. Aberrations in these planes broaden and translate the PSF laterally when the optical scanners (placed in pupil conjugate planes) move. This is commonly termed "beam wandering." Both these effects degrade the wavefront measurement and correction, and therefore the AO performance. Figure 2 shows the spot diagrams corresponding to the point along the optical axis at the pupil plane for the 9 orientations of the optical scanner considered in Fig. 1. The large colored spot diagrams on the left illustrate how the large astigmatism component of the planar configuration not only enlarges the actual spots, but also displaces them (beam wandering). Folding the telescope out of the plane onto the orthogonal configuration results in more compact spot diagrams (i.e. lower wavefront RMS), and a significant reduction in beam wandering. The corresponding wavefront RMS ignoring the beam wandering is $\lambda/13$ for the planar configuration and $\lambda/56$ for the orthogonal one, which is a comparable improvement to that observed in the retinal plane.

Fig. 2. Spot diagrams corresponding to the pupil plane of a 1:1 off-axis reflective telescope that consists of two spherical mirrors in a planar configuration (left) and orthogonal configuration (right). The black circles correspond to the first minimum of the Airy disk.

3. The need for aberration correction over a vergence range

BAOSOs can be grouped into two categories, depending on whether the illumination is focused onto one or multiple retinal layers simultaneously. Among the former one finds reflectance imaging [8,9,11] and OCT [4–6,14–16], while the latter includes dual-imaging modalities, such as fluorescence imaging, in which one of the retinal layers being imaged is used as a registration signal to compensate for eye motion in a second imaging channel [10,12].

When focusing the illumination onto a single retinal layer, both the illumination and scattered or fluorescent light can propagate through the optical system with a single vergence, provided the longitudinal chromatic aberration (LCA) of the eye is compensated with an achromatizing lens placed in the pupil plane of the eye. In order to avoid back reflections, such achromatizing lenses have been placed in pupil conjugate planes other than that of the eye [14–16], and therefore each wavelength propagates through the optical system between the achromatizing lens and the eye with different vergences determined by the LCA. When trying to image multiple retinal layers simultaneously, a vergence adjustment different from that of the LCA of the eye is required. Therefore, unless a tunable LCA correcting device is placed in the pupil plane of the eye, it will be unavoidable to have different beams of light propagating through the reflective optical system with different vergences. Beams of light propagating through an optical system with different vergences will be affected by different aberrations. This is because rays of light corresponding to beams propagating with different vergences will reach different areas of the optical elements, and also impinge on the surfaces with different angles of incidence, as illustrated in the refractive afocal telescope shown on Fig. 3.

#143934 - $15.00 USD Received 10 Mar 2011; revised 22 Apr 2011; accepted 22 Apr 2011; pub. 27 May 2011

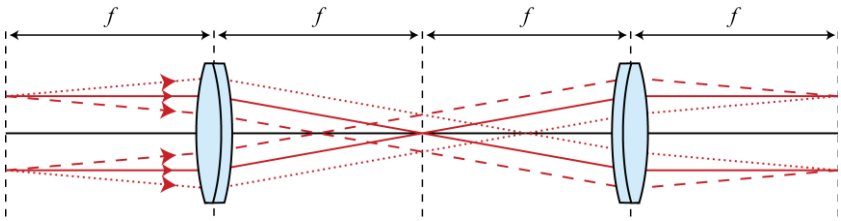

Fig. 3. Afocal 1:1 telescope in which *f* denotes the focal length of the lenses. The three beams entering the telescope with negative, null and positive vergences are indicated with dotted, solid and dashed lines respectively.

There are two factors that should be considered when specifying the BAOSO vergence range: the thickness of the retina, and the LCA of the eye (both measured in diopters). The instrument described herein is designed to simultaneously image the retina and the nerve fiber layer (NFL) in human subjects with a combined thickness of approximately 360 μm [17]. Using eye models such as the Gullstrand #2 simplified and the Emsley reduced [18], the retinal thickness can be translated to 1.0 and 0.9 D vergences, respectively, as shown on the left panel of Fig. 4. Work by Thibos *et al*. [19] and Fernández *et al*. [20] provide quantitative estimates of the LCA of the human eye over the visible and near infrared spectral regions. The plot on the right panel of Fig. 4 combines both LCA models, showing a vergence range of 1.6 D over the 450-850 nm wavelength range to be considered for the instrument described below. Therefore, for the BAOSO to be able to image any combination of retinal layers with the specified wavelength range without any achromatizing element, it should be diffraction limited over at least a 2.6 D vergence range. The BAOSO in this work was designed to cope with a 3 D vergence range.

4. Optical design of a broadband adaptive optics scanning ophthalmoscope

The steps in the next five paragraphs should be considered to achieve the best optical performance allowed by the system specifications and mechanical mounts when designing a BAOSO using off-axis afocal telescopes formed by pairs of spherical mirrors.

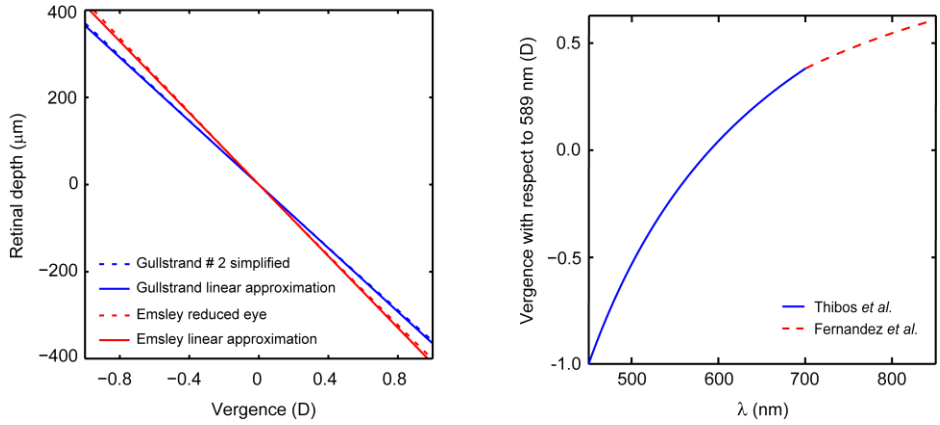

Fig. 4. Retinal depth dependence with the vergence of the beam entering the eye (left), according to two simple model eyes. The plot on the right shows two longitudinal chromatic aberration models for the human eye.

First, select the magnification of the afocal telescopes that relay the pupil plane of the eye as close to 1:1 as permitted by the optical scanners, wavefront corrector and other optical elements to be placed in the planes conjugate to the pupil of the eye. As indicated by Gómez-Vieyra *et al.* [13], this is the optimal magnification for simultaneous compensation of astigmatism in the retinal and pupil conjugate planes when using a non-planar telescope configuration.

#143934 - $15.00 USD Received 10 Mar 2011; revised 22 Apr 2011; accepted 22 Apr 2011; pub. 27 May 2011

In principle, a large FOV is desirable in ophthalmic AO instruments for surveying the retina for features of interest and, more importantly, for establishing the retinal location being imaged with high resolution (i.e. small FOV). However, the largest FOV to be used in the BAOSO defines the minimum angle of incidence of the optical axis on each of the spherical mirrors, and the larger these angles are the poorer the optical performance of the optical system will be [13]. Therefore, a trade-off should be made between the size of the largest FOV to be used and the minimum optical performance that is acceptable.

Careful consideration should be given to the order of the optical elements placed in the pupil planes. For example, the optical performance of the system will be best when the wavefront corrector is in the pupil plane closest to the eye. If there are multiple pupil planes to be used for wavefront correction (e.g. trial lenses or large and small stroke deformable mirrors), the correcting device that provides the largest correction in terms of defocus and astigmatism should be placed in the pupil plane closest to the eye. In this way, the area of the optical elements being used is kept to a minimum. Based on the same principle, if the beam diameter at both optical scanners is identical, the one with the larger FOV should be in the pupil plane closer to the eye.

The Coddington equations indicate that the astigmatism introduced by the off-axis use of a spherical mirror varies linearly with the focal length of the mirror and quadratically with the angle of incidence for small angles. Therefore, minimizing the angles of incidence takes precedence over minimizing the focal length of the spherical mirrors. Given the dimensions of the elements to be placed in the pupil planes and their mechanical mounts, the angles of incidence on the spherical mirrors can be reduced by increasing their focal length. In fact, doubling the focal length of the mirrors would cut the astigmatism in half, indicating that the largest acceptable dimensions for the optical setup, determined by the focal lengths of the spherical mirrors, should be selected.

Once the spherical mirrors have been specified, the optical setup should be designed by both using the smallest possible angles of incidence on the spherical mirrors and folding each telescope as close to the orthogonal configuration as mechanical restrictions allow, in order to minimize astigmatism. Then, and provided mechanical limitations allow it, each telescope could be rigidly rotated in space to reduce coma [13].

A BAOSO, sketched in Fig. 5, was designed following the steps described above with the following specifications: 2.45° as the largest horizontal FOV, 5.75° as the largest vertical FOV and 7.5 mm beam diameter at the eye. Optical scanning is achieved using an SC-30 resonant galvanometric optical scanner from Electro-Optical Products Corp. (Fresh Meadows, New York, USA), and a VM2500 + non-resonant galvanometric optical scanner from GSI Group Corp (Billerica, Massachusetts, USA). The wavefront sensor is a custom Shack-Hartman sensor that uses a Rolera-XR camera from QImaging (Surrey, British Columbia, Canada) and a 203 μm pitch, 7.8 mm focal length lenslet array from Adaptive Optics Associates (Cambridge, Massachusetts, USA). The wavefront correction is performed using a Hi-speed DM97 deformable mirror from ALPAO S.A.S. (Biviers, Grenoble, France). The spherical mirrors used are from CVI-Melles Griot (Albuquerque, New Mexico, USA), and JML Optical Industries Inc. (Rochester, New York, USA). The light sources used are: an 850 nm laser diode from Qphotonics (Ann Arbor, Michigan, USA), a 680 nm superluminescent diode (SLD) with 8.5 nm full-width half-maximum (FWHM) bandwidth from Superlum Ireland (Carrigtwohill, County Cork, Ireland), and a 796 nm SLD with 14 nm FWHM bandwidth from Inphenix Inc. (Livermore, California, USA). Light from all three light sources was delivered to the instrument through single-mode fibers. Light scattered by the retina was detected using photomultiplier modules H7422-40 and −50 from Hamamatsu Corporation (Bridgewater, New Jersey, USA). The PMT output is amplified and converted to voltage using transimpedance amplifiers HCA-10M-100K from Femto Messtechnik GmbH. (Berlin, Germany), and then inverted with in-house electronics before digitization using a Helios eA framegrabber from Matrox International Corporation (Dorval, Quebec, Canada).

#143934 - $15.00 USD Received 10 Mar 2011; revised 22 Apr 2011; accepted 22 Apr 2011; pub. 27 May 2011

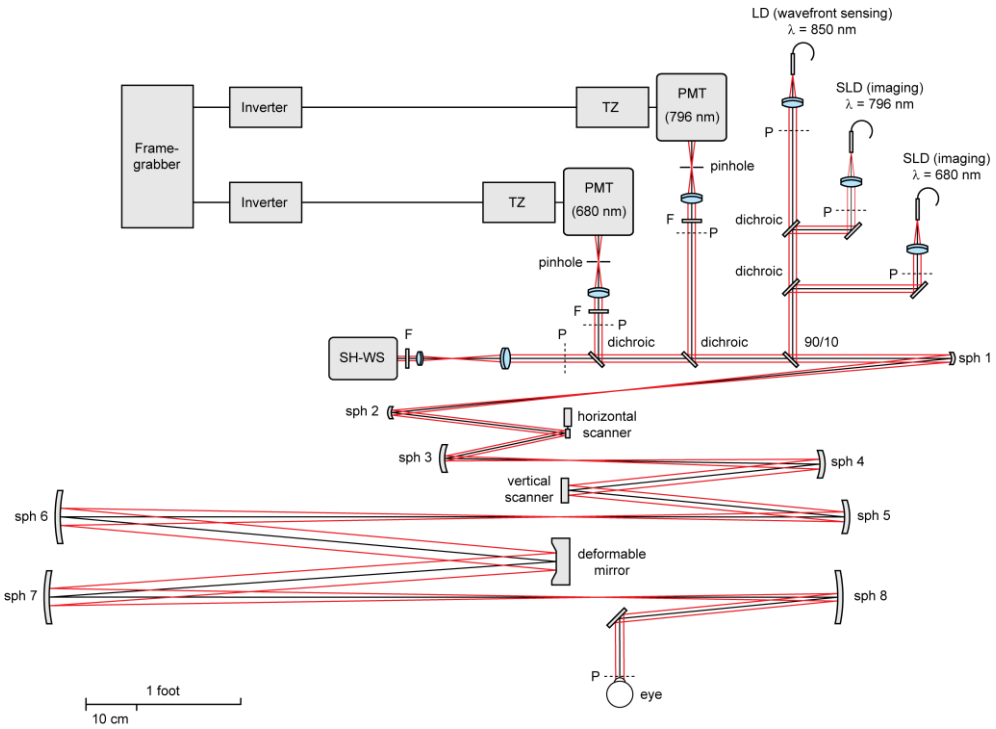

Fig. 5. Broadband adaptive optics scanning ophthalmoscope setup flattened for clarity. PMT stands for photomultiplier, TZ for transimpedance amplifier, LD for laser diode, SLD for superluminescent diode, SH-WS for Shack-Hartmann wavefront sensor, sph for spherical mirror and F for interferometric band pass filter. The letter P indicates the pupil conjugate planes, in addition to the ones corresponding to the deformable mirror, the optical scanners and the SH-WS.

The design of the reflective part of the BAOSO is solely defined by the focal lengths of the spherical mirrors and the angles of incidence onto these and the reflective elements in the pupil planes. The optical performance at the retinal conjugate plane was evaluated by calculating the power mean with exponent 2 of the wavefront RMS over 9 points uniformly distributed over the field of view and over one (0.0 D) or three (–1.5, 0.0 and +1.5 D) vergences at the pupil of the eye. Similarly, the optical quality in the pupil plane of the eye was evaluated by calculating the wavefront RMS for a single point along the optical axis for each of the 9 orientations of the optical scanners that correspond to the 9 retinal locations being considered. It is important to note that determining the aperture stop location for evaluating the image quality in pupil planes is not trivial. It would be desirable to select it so that the area of the mirrors used by the rays traced by ZEMAX is similar to that used by the rays traced when determining the image quality at the retinal conjugate planes. With this in mind, we selected the area illuminated by the imaging rays over the first spherical mirror of the system (i.e. the furthest from the eye) as the aperture stop, which was 7.87 mm in diameter. All wavefront RMS values were evaluated in terms of the shortest wavelength consistent with the coating of the reflective optical elements in the system (450 nm). Finally, optimization in ZEMAX was used to determine the defocus and astigmatism, applied by the deformable mirror, necessary to minimize the overall wavefront RMS for all vergences and points over the field of view without affecting the image quality in the pupil conjugate planes. Note that this optimization process uses only one deformable mirror shape that is applied to all points on the field of view and all the vergences. In practice, the deformable mirror will correct more aberrations than just those two, and therefore the results presented below for the retinal plane are arguably conservative.

#143934 - $15.00 USD Received 10 Mar 2011; revised 22 Apr 2011; accepted 22 Apr 2011; pub. 27 May 2011

Table 1 shows the angles of incidence along the x- and y-axis in the proposed design. The telescopes formed by the first, third and fourth spherical mirror pairs are folded at 90°, which, as mentioned above, is the configuration with the lowest astigmatism. Due to the dimensions of the mechanical mounts, the second telescope could only be folded at 63° without increasing the angles of incidence. The RMS values for the retina and pupil conjugate planes over the largest FOV for the instrument (2.45° × 5.75°) are λ/22 and λ/11 respectively.

Table 1. Focal length and angles of incidence onto the reflective optical elements of the BAOSO

Optical element	Focal length (mm)	I_x (deg)	I_y (deg)
Spherical mirror # 1	750	1.60	0.00
Spherical mirror # 2	375	0.00	–0.90
Horizontal scanner	-	0.00	2.30
Spherical mirror # 3	400	0.00	0.80
Spherical mirror # 4	800	1.70	–0.85
Vertical scanner	-	–3.85	–3.85
Spherical mirror # 5	550	1.40	0.00
Spherical mirror # 6	1000	0.00	–1.85
Deformable mirror	-	–0.25	3.85
Spherical mirror # 7	1000	0.00	2.30
Spherical mirror # 8	550	3.20	0.00

Table 2 summarizes the performance for two smaller FOVs that are comparable to the isoplanatic patch of the eye [21]. The wavefront RMS for each field of view is always lowest for emmetropic subjects (i.e. 0.0 D prescription) irrespective of the vergence range. When either the vergence range considered and/or the absolute value of the subject's prescription increases the wavefront RMS increases. The prescription values shown in Table 2 indicate the extremes of the range over which the system's performance is diffraction limited. For the selected FOVs, the indicated prescription range corresponds to more than 75% of the population [22]. Moreover, if a wavelength longer than 450 nm is used for imaging, as is the case in the next section, then the prescription range over which diffraction limited performance can be achieved is larger than the values reported in Table 2. The wavefront RMS values at the pupil plane of the eye for 1.0° and 1.5° are λ/18 and λ/16, respectively, which correspond to diffraction limited performance according to Maréchal's criterion of wavefront RMS lower than λ/14.

Table 2. Wavefront RMS (λ = 450 nm) for different BAOSO FOV and vergences. Positive values in the subject's prescription column correspond to myopic subjects.

FOV (deg)	Vergences @ eye (D)	Subject's prescription (D)	RMS (λ)
1.5	–1.5, 0.0, +1.5	5.5	1/14
		0.0	1/36
		–3.0	1/15
1.5	0.0	6.5	1/14
		0.0	1/83
		–4.5	1/16
1.0	–1.5, 0.0, +1.5	6.5	1/14
		0.0	1/38
		–4.0	1/14
1.0	0.0	7.5	1/14
		0.0	1/125
		–6.0	1/14

#143934 - $15.00 USD Received 10 Mar 2011; revised 22 Apr 2011; accepted 22 Apr 2011; pub. 27 May 2011

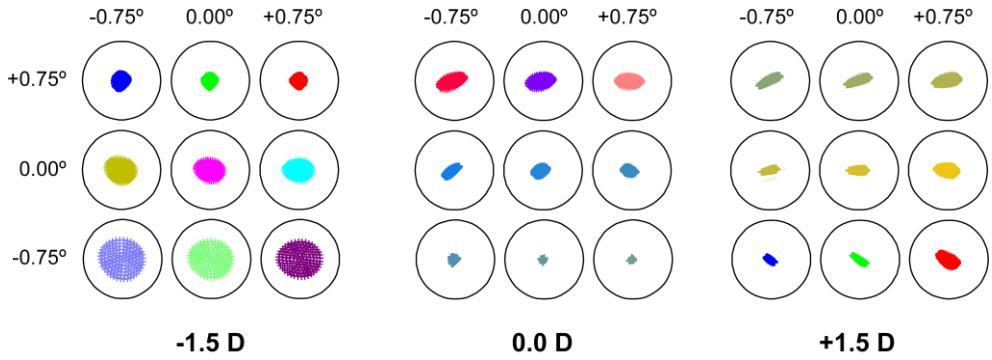

Fig. 6. Spot diagram for all 27 BAOSO configurations evaluated, grouped according to the vergence. Note that all configurations are diffraction limited for 450 nm wavelength over a 1.5° FOV. The radius of the Airy disk indicated by the black circles is 1.3 μm.

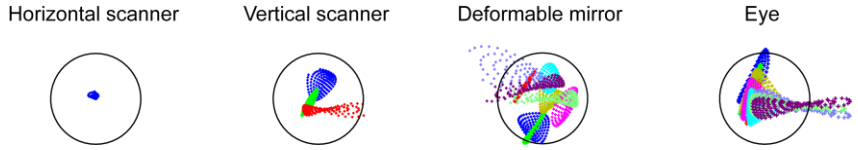

Fig. 7. Spot diagrams for all 4 pupil planes of the BAOSO for 450 nm wavelength over a 1.5° FOV, assuming a point source at the pupil plane in front of the Shack-Hartman wavefront sensor telescope. The black circles represent the Airy disk.

Finally, spot diagrams in the retinal plane for all three vergences considered for a 1.5° FOV and an emmetropic subject are displayed in Fig. 6. Figure 7 shows the spot diagrams corresponding to all four intermediate pupil planes for the same field of view. Note that these pupil plane spot diagrams are independent of beam vergence or subject prescription.

5. Experimental evaluation: human imaging

In order to demonstrate the optical performance of the BAOSO, reflectance images were recorded in a 27-year-old, male emmetrope with slightly longer than average axial length, 24.64 mm [23]. Written informed consent was obtained after the nature and possible risks of the study were explained. The eye to be imaged was dilated and cycloplegia was topically induced with one drop of a combination of phenylephrine hydrochloride (2.5%) and tropicamide (1%). The subject was aligned and stabilized with the use of a dental impression on a bite bar. The light exposure was kept below ANSI standard maximum permissible exposure at all times [24,25].

In order to illustrate the optical performance at different vergences, the vergences of the imaging channels were purposely adjusted to add to the focus shift due to the LCA. The vergences of the imaging sources at the eye with respect to the 850 nm wavefront sensing source were +0.32 D for the 796 nm and −0.44 D for the 680 nm channels. Because of the LCA between the two imaging channels, the 0.76D of relative vergence at the pupil of the eye translates in a 0.53 D focus difference between both channels at the retina.

Sequences of images were recorded using a FOV of approximately 0.75°. The image stretching resulting from the sinusoidal motion of the resonant optical scanner was compensated by estimating the distortion from images of a Ronchi ruling, and then re-sampling the images over a grid of equally spaced pixels. Eye motions artifacts were removed and then a number of registered frames were averaged, in order to increase signal to noise ratio using custom software [26].

Figures 8 and 9 show registered averages of images of the full foveal cone photoreceptor mosaic. Typically, most photoreceptor images are displayed with a linear relation between recorded image intensity and display gray scale value. Because of the large variations

#143934 - $15.00 USD Received 10 Mar 2011; revised 22 Apr 2011; accepted 22 Apr 2011; pub. 27 May 2011

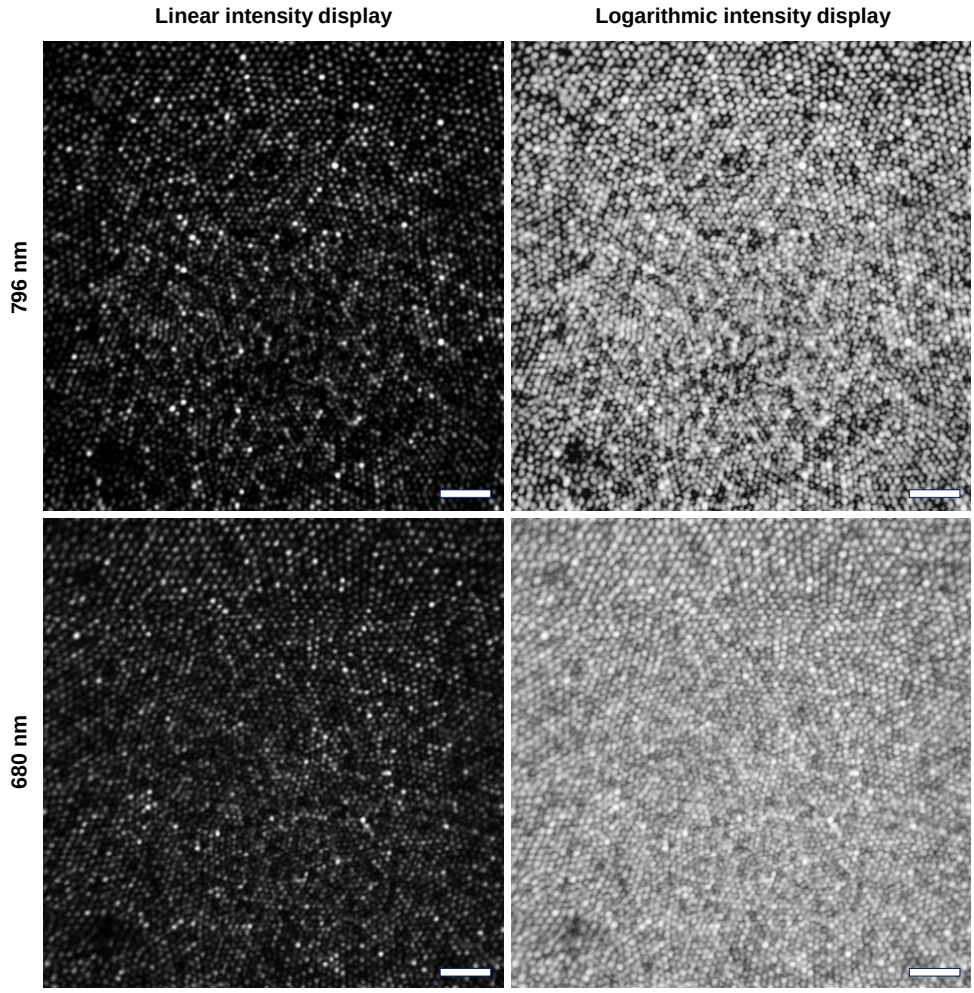

Fig. 8. Human photoreceptor mosaic at the foveal center, recorded with the BAOSO. The top images were recorded with a 796 nm SLD and a 0.6 Airy disk confocal pinhole size, while the bottom ones were obtained using a 680 nm SLD and a 0.4 Airy disk confocal pinhole. The images on the left display the image intensity using a linear gray scale mapping, while the images on the right are displayed using a logarithmic gray scale transformation. The scale bars are 20 μm across.

observed in photoreceptor brightness, we propose displaying these maps using a logarithmic gray scale mapping, as used in ophthalmic OCT, for visualization purposes. It should be noted that when scaling the image intensity using a logarithmic transformation, the PSF increases its FWHM by 80%, as shown in Fig. 10, with the subsequent reduction in resolution. Despite such loss of resolution, all the foveal cones in Figs. 8 and 9 can be resolved.

6. Conclusions

A broadband adaptive optics scanning ophthalmoscope consisting of four reflective afocal telescopes was presented. By folding these telescopes in non-planar configurations, the astigmatism affecting the pupil and image conjugate planes were simultaneously reduced to the extent that image quality in both sets of planes was limited by diffraction over a 3 D vergence range, and over a 10 D prescription range for a 1.0° FOV for 450 nm light. An added benefit of this astigmatism correction was the near total removal of beam wandering. The

#143934 - $15.00 USD Received 10 Mar 2011; revised 22 Apr 2011; accepted 22 Apr 2011; pub. 27 May 2011

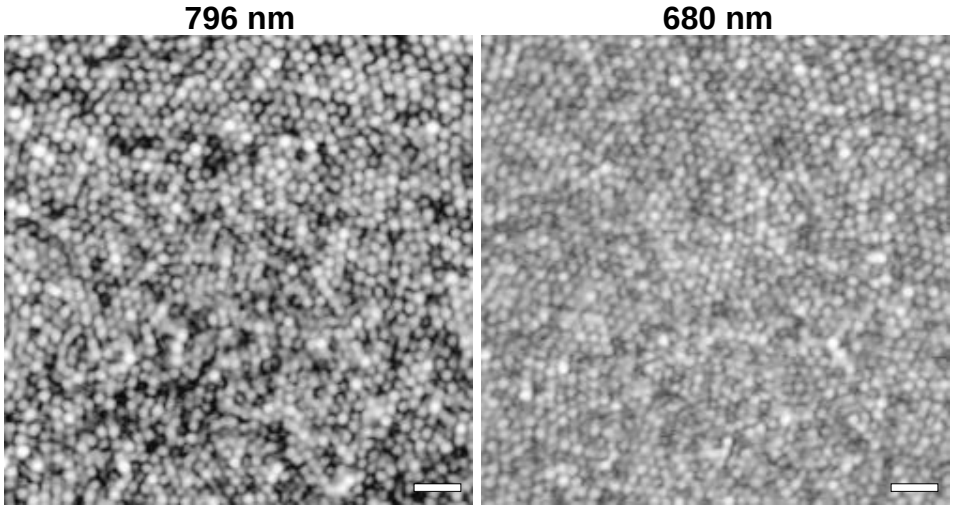

Fig. 9. Enlarged version of the photoreceptor mosaic shown in Fig. 8, showing the smallest foveal cones. The scale bars are 10 μm across.

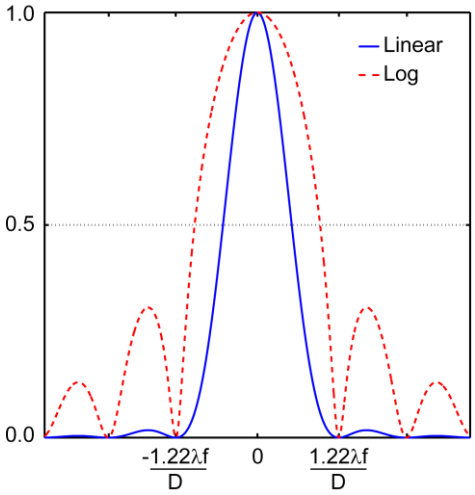

Fig. 10. Cross section of an Airy disk and its logarithm, which is 80% wider.

specified vergence range allows the use of any broadband light source(s) in the 450-850 nm wavelength range for simultaneous imaging of any combination of retinal layers. The diffraction limited performance over such a large vergence and prescription range comes at the price of a physically large optical setup that, without folding mirrors, is over 1.75 m long. The size of the instrument could be reduced by using a two-dimensional resonant optical scanner and a deformable mirror with a 7-8 mm diameter pupil. In fact, using longer wavelengths and 1:1 magnification telescopes, an instrument with comparable prescription correction range and less than a third of the size could be built [27].

The performance of the optical setup was tested by imaging the fovea of a human subject using two light sources that propagated through the systems with a relative vergence of 0.76 D. The images, successfully resolve the smallest cone photoreceptors at the foveal center.

Finally, the logarithmic display for visualization of the photoreceptor mosaic is proposed, with the caveat of an associated 80% PSF broadening.

#143934 - $15.00 USD Received 10 Mar 2011; revised 22 Apr 2011; accepted 22 Apr 2011; pub. 27 May 2011

Acknowledgments

Alfredo Dubra-Suarez, Ph.D., holds a Career Award at the Scientific Interface from the Burroughs Welcome Fund. This research was supported financially by the National Institute for Health, Bethesda, Maryland (NIH EY014375), and Research to Prevent Blindness. The inverting electronics for the PMT signals were designed and built by Ted Twietmeyer, and the image acquisition software and optical scanners control were developed by Zach Harvey. We are very grateful to Ying Geng, Ben Masella, Robin Sharma, and Drew Scoles for helpful discussion and editing of this manuscript.

#143934 - $15.00 USD Received 10 Mar 2011; revised 22 Apr 2011; accepted 22 Apr 2011; pub. 27 May 2011